Isospin effects in elastic proton-nucleus scattering

C. R. Chinn*
Service de Physique et Techniques Nucléaires, Center d'Etudes de Bruyères-le-Châtel, B.P. No. 12, 91680 Bruyères-le-Châtel, France

Ch. Elster
Institute of Nuclear and Particle Physics, and Department of Physics, Ohio University, Athens, Ohio 45701

R. M. Thaler
Los Alamos National Laboratory, Los Alamos, New Mexico 87545 and Case Western Reserve University, Cleveland, Ohio 44106

(Received 17 December 1992)

Isovector effects in proton-nucleus elastic scattering at medium energies are studied. The accuracy of the Kerman-McManus-Thaler isospin averaging procedure is found to be very good for nuclei larger than ^{4}He. Studies of ^{40}Ca and ^{208}Pb suggest that the surface neutrons may be pulled in somewhat relative to the protons, although uncertainties in the detailed applicability of the present truncation of the multiple scattering treatment render firm conclusions premature.

PAC number(s): 25.40.Cm

I. INTRODUCTION

Despite the recent progress that has been made in the multiple scattering theory (MST) treatment of nucleon-nucleus elastic scattering (for example the full folding of the off-shell nuclear density matrix [1–3] and the treatment of the Coulomb interaction in momentum space [4]), there remain unresolved questions even within the first-order MST. These questions especially concern the assumptions in the process through which the free nucleon-nucleon (NN) t matrix is introduced into the theory. A consistent development of the isovector degrees of freedom may help clarify some of the unresolved issues; for example, the complete folding of the fully off-shell free NN t matrix and the fully off-shell density matrix clearly involves isovector degrees of freedom. The renewed interest in neutron degrees of freedom has been in part inspired by recent measurements of the total elastic neutron-nucleus cross section for a variety of nuclei [5] as well as recent theoretical calculations in the construction of Dirac neutron-nucleus optical potentials [6, 7].

In this paper the isovector degrees of freedom are discussed from two different points of view. First, isovector effects intrinsic to the multiple scattering expansion are laid out within the framework of the Watson multiple scattering expansion [8]. The inclusion of isovector effects in the Kerman-McManus-Thaler (KMT) formalism is somewhat tedious [9], whereas in the first-order Watson multiple scattering form the neutrons and protons can be treated explicitly without any difficulty. This treatment is discussed and the resulting effects with identical neutron and proton distributions are shown in Sec. II. Second, differences in the matter distribution of protons and neutrons may also be interpreted as isovector effects. In Sec. III, the formalism presented in the previous section is used to look at the impact of differences in the neutron density on elastic proton scattering. Although the proton density distribution is very well determined from electron scattering data [10], this is certainly not the case for the neutron distribution. It has been recently suggested that a better determination of the neutron density would be very interesting for the case of atomic parity nonconserving analysis of the standard electroweak model [11]. With the advent of more precise neutron scattering experiments, the uncertainties resulting from the lack of understanding of the neutron densities are also becoming important questions in elastic neutron scattering. Here, we examine the extent of these ambiguities by looking at how changes in the neutron density distributions are reflected in the elastic proton-nucleus observables.

II. ISOVECTOR DEGREES OF FREEDOM IN THE MST

The two most familiar approaches for the construction of a first-order optical potential for nucleon-nucleus elastic scattering are those of Watson [8] and Kerman-McManus-Thaler (KMT) [12]. The Watson first-order multiple scattering series requires us first to solve a preliminary integral equation to obtain the optical potential, which is then taken as input to a Lippmann-Schwinger-type integral equation. The KMT formalism assumes that the NN t-matrix interactions are identical for all projectile-target nucleon situations. This allows us to

*Present address: Department of Physics and Astronomy, Vanderbilt University, Nashville, TN 37235.

combine the preliminary integral equation for the optical potential with the Lippmann-Schwinger equation into a single integral equation with the familiar $(A-1)/A$ scaling factors. The assumption of identical interactions in the KMT derivation makes it awkward to treat the isovector differences in the nucleon-nucleon interaction. An estimate of the isovector corrections within the KMT formalism has been given in Ref. [9]. Since the Watson formalism does not assume identical proton-proton and neutron-proton interactions, the treatment of the isovector degrees of freedom is particularly straightforward within this framework. Throughout this article any reference to a KMT optical potential implies the use of an isospin averaged NN t matrix.

To demonstrate the treatment of the isovector degrees of freedom, the Watson multiple scattering series is summarized briefly. The input into the Lippmann-Schwinger equation is defined to be the Watson optical potential:

$$U^W = \sum_{i=1}^{A} \left[\tau_i + \tau_i G_0 \mathrm{Q} \sum_{j \neq i} \tau_j + \cdots \right] \tag{1}$$

$$\approx \sum_{i=1}^{A} \tau_i, \tag{2}$$

where

$$\tau_i = v_{0i} + v_{0i} G_0 \, \mathrm{Q} \, \tau_i. \tag{3}$$

The first-order or single scattering approximation is defined in Eq. (2). The nucleon-nucleon interaction is given by the two-body potentials v_{0i}. The projector Q is given by $\mathrm{Q} = 1 - P$, where $P = |\psi_A\rangle\langle\psi_A|$ projects onto the nuclear ground state. The free propagator in the nuclear medium is defined as $G_0^{-1} = E - h_0 - H_A$. After some algebraic manipulation an alternative expression for the "Watson" τ_i is easily seen to be

$$\tau_i = \tilde{t}_i - \tilde{t}_i \, P \, G_0 \, \tau_i, \tag{4}$$

where

$$\tilde{t}_i = v_{0i} + v_{0i} \, G_0 \, \tilde{t}_i. \tag{5}$$

The operator $\tilde{t}_i$ does not contain the projector Q and is usually taken to be the free NN t matrix, t_i, which is obtained as a solution of the integral equation

$$t_i = v_{0i} + v_{0i} \, g_0 \, t_i. \tag{6}$$

The free two-nucleon propagator g_0^{-1} is given by

$$g_0^{-1} = E' - h_0 - h_i. \tag{7}$$

The preliminary integral equation mentioned earlier for obtaining the Watson optical potential is given by Eq. (4), and is straightforward to solve. Since the τ_i's are expressed separately for each i, no assumption about the isospin character of the NN interaction is made at this stage. The proton-proton and proton-neutron interactions are treated independently in Eq. (4). Therefore, the subsequent optical potential is the sum of two different contributions:

$$U^W = \sum_{i=1}^{Z} \tau_{p,i} + \sum_{i=1}^{N} \tau_{n,i} = Z \, \tau_p + N \, \tau_n. \tag{8}$$

As is obvious from Eq. (8), the isovector character of τ_p and τ_n as well as their corresponding convolution with the proton and neutron distributions is taken into account in a completely consistent fashion.

In Figs. 1 and 2 the effects of various treatments of the isovector character of the optical potential are shown for elastic proton scattering from ^{4}He at 200 MeV laboratory energy. The solid line in Fig. 1 represents a consistent calculation of the Watson optical potential according to Eq. (8), whereas the calculation given by the dotted line omits the step of solving the integral equation [Eq. (4)] for the Watson optical potential. In short, the dotted line represents setting $\tau_i = \tilde{t}_i = t_i$ in Eq. (4) or equivalently setting $(A-1)/A = 1$ in the KMT formalism. For scattering from a light nucleus like ^{4}He this approximation is quite drastic, as is seen in the first minima in the spin observables A_y and Q. The inadequacy of this approximation was long ago pointed out in Ref. [13]. In Fig. 2 a calculation with the Watson optical potential [Eq. (8), solid line] is compared with a calculation within the KMT formalism employing an isospin averaged NN interaction. Though for small scattering angles the isospin averaged NN interaction seems to be quite a good approximation, for scattering angles larger than 60° this is certainly not the case. A similar observation of the shortcoming of the KMT isospin averaging was made

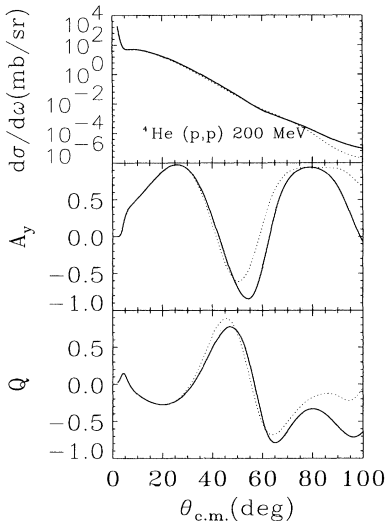

FIG. 1. The angular distribution of the differential cross section (σ), analyzing power (A_y), and spin rotation function (Q) for elastic proton scattering from ^{4}He at 200 MeV laboratory energy. The calculations are performed with a first-order optical potential obtained from the full Bonn interaction [20] in the optimum factorized form. The solid curve represents the calculation within the Watson formulation, whereas the dotted line omits the solution of the integral equation for the Watson optical potential.

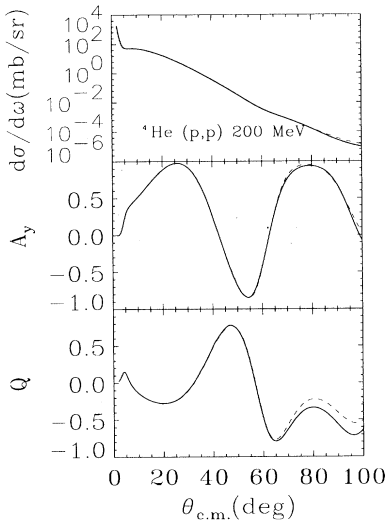

FIG. 2. Same as Fig. 1. The solid curve represents the calculation within the Watson formulation, whereas the dashed line employs a first-order KMT optical potential.

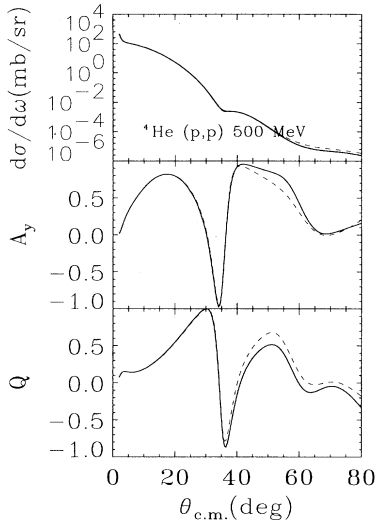

FIG. 3. The observables σ, A_y, and Q for elastic proton scattering from ^{4}He at 500 MeV laboratory energy. The solid line represents a calculation with a Watson first-order optical potential, whereas the dashed line is obtained with a KMT first-order optical potential.

in Ref. [14], where the scattering of pions from ^{4}He was investigated.

For the clarity of our argument, we have assumed the proton and neutron distributions to be equal in the above described calculations. Thus, Figs. 1 and 2 display the accuracy of two different approximations to the Watson first-order optical potential, namely assuming $\tau_i = t_i$ (Fig. 1) and the KMT isospin average of the NN interaction (Fig. 2). In both calculations the proton density distribution is taken from a microscopic Hartree-Fock-Bogoliubov (HFB) calculation of Ref. [15], which uses the Gogny D1S finite range effective interaction [16]. The neutron distribution is taken to be equal to the proton distribution.

To calculate the elastic scattering observables, we use the optimum factorized or "off-shell $t\rho$" approximation [17], which has been found to be a good approximation to the full-folding integral in the energy regime between 200 and 800 MeV [1, 3]. As shown in Eq. (7) the free NN t matrix has to be evaluated at an appropriate energy E'. In principle, this energy should be the beam energy minus the kinetic energy of the center of mass of the interacting pair less the binding energy of the struck particle [18]. Since in practice the relevant-matrix elements do not depend strongly on this variable [19], E' is set to the two-body energy corresponding to free NN scattering at the beam energy. It is to be understood that all spin sums are performed under the usual assumption of a spin saturated target, thus reducing the required NN t-matrix elements to the spin-independent component (corresponding to Wolfenstein amplitude A) and the spin-orbit component (corresponding to Wolfenstein amplitude C). All scattering calculations presented here contain an additional factor in the optical potential to account for the transformation of the NN t matrix from the two-nucleon c.m. frame to the nucleon-nucleus c.m. frame. This Møller factor is obtained in a manner discussed in Ref. [17]. At 200 MeV we employ the NN t matrix from the full Bonn interaction [20]. The Coulomb interaction is included in all three calculations using the method described in Ref. [4].

For our scattering calculation at 500 MeV we start from an extension of the Bonn meson exchange interaction above pion production threshold, which is described in more detail in Ref. [21]. The elastic scattering observables for proton scattering from ^{4}He at 500 MeV are displayed in Fig. 3, just as in Fig. 2. Again, the solid line represents a calculation of the Watson optical potential

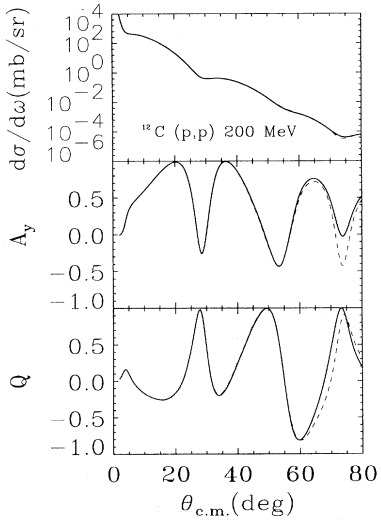

FIG. 4. The observables σ, A_y, and Q for elastic proton scattering from ^{12}C at 200 MeV laboratory energy. The solid curve corresponds to the first-order Watson calculation. The dashed curve corresponds to the KMT calculation, which averages over the isovector degrees of freedom.

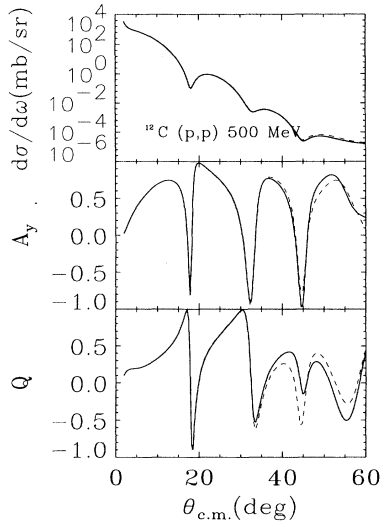

FIG. 5. The observables σ, A_y, and Q for elastic proton scattering from ^{12}C at 500 MeV laboratory energy. The notation corresponds to that in Fig. 4.

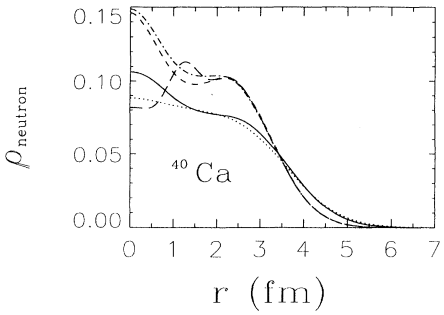

FIG. 6. Neutron density distributions in coordinate space for ^{40}Ca as a function of the nuclear radius. The solid curve is from a microscopic HFB calculation [16], whereas the short-dashed, dash-dotted, and long-dashed curves are volume conserving modifications thereof, and define cases (a), (b), and (c), respectively. The dotted line represents the proton distribution as given by a Sum-of-Gaussians fit [10] to the experimentally determined proton distribution.

according to Eq. (8), whereas the dashed line shows the KMT isospin averaged optical potential. After the first minimum, at angles larger than ~40°, the KMT approximation begins to deviate from the Watson result.

Studying larger nuclei, we find that the isovector effects discussed here become smaller. In Figs. 4 and 5 we show elastic scattering observables for proton scattering from ^{12}C at 200 and 500 MeV. The isovector effects due to the KMT approximation (dashed line) to the Watson optical potential (solid line) are small and the KMT average is quite accurate even for larger scattering angles. Beyond ^{12}C in the periodic table, our calculations indicate that for energies larger than 200 MeV there are no differences which would be visible in graphs similar to Figs. 4 and 5. For investigations at energies less than 200 MeV, it may be necessary to consider these isovector effects even for heavier nuclei.

III. ELASTIC NEUTRON AND PROTON SCATTERING

In the previous section we took care to make the neutron and proton densities identical in order to isolate the effect due to the difference between the isospin 0 and 1 parts of the NN interactions. The isospin differences between the Watson and KMT formulation of the MST due to the NN interaction are negligible in heavy nuclei, even if the neutron and proton distributions are not identical. We now wish to look at effects arising from possible differences between the neutron and proton distributions. We present the results of this study as a series of plots of scattering observables, Figs. 9 through 12. In these figures we show the differential cross section σ, the polarization A_y, and the spin rotation parameter Q for proton elastic scattering from ^{40}Ca and ^{208}Pb as calculated with various densities. The proton density is taken to be a 24 parameter Sum-of-Gaussian fit to electron scattering data [10,22]. We show results for the neutron distribution set to be equal to the proton distribution, a neutron distribution obtained from a microscopic HFB calculation [16] along with several different *ad hoc* neutron densities. These comparisons represent an indication of the sensitivity of the elastic scattering observables to the neutron densities employed. The corresponding modified neutron distributions are shown in Fig. 6 for ^{40}Ca and Figs. 7 and 8 for ^{208}Pb. It must be strongly emphasized that these calculations do not pretend to be a study whereby we hope to pin down the neutron distribution from proton elastic scattering. In this work we are exploring the sensitivity of the observables due to changes in the neutron distribution. These studies are an essential preliminary to the proper inclusion of higher-order effects (including medium modifications in the propagator) in elastic scattering.

We note that all the figures indicate a lack of sensitivity

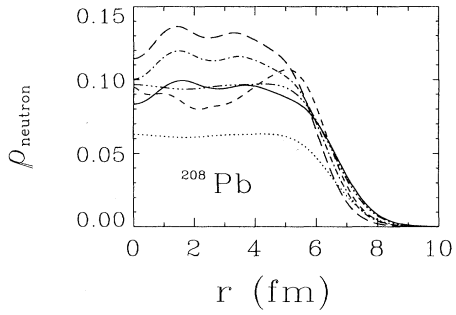

FIG. 7. Neutron density distributions for ^{208}Pb as a function of the nuclear radius. The solid curve is from a microscopic HFB calculation [16], whereas the short-dashed, dash-dotted, and long-dashed curves are volume conserving modifications thereof, and define cases (a), (b), and (c), respectively. The dotted line represents the proton distribution as given by a Sum-of-Gaussians fit to the experimentally determined proton distribution [22]. The dash-dot-dotted line represents the neutron distribution obtained by scaling the proton distribution by the factor N/Z.

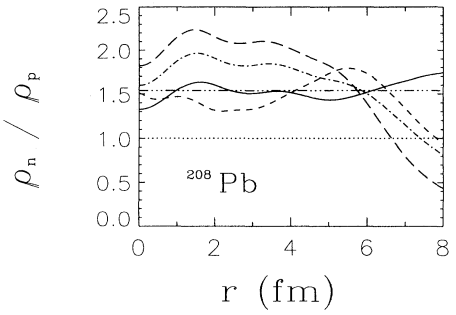

FIG. 8. The ratio $R = \rho_n/\rho_p$ of the neutron density to the proton density. The lines are coded as in Fig. 7.

to the density in the central region of the target nucleus. This inability of the proton to probe the interior of the nucleus in the regime under discussion has been known for a very long time and is not meant to be a new result of the present investigation. If we define the exterior region by $r > R_A = 1.1A^{1/3}$ (where $R_{40} = 3.4$ fm and $R_{208} = 6.5$ fm), we observe that in that region the HFB neutron and proton distributions (appropriately scaled) are nearly identical for both nuclei under consideration. The observables are likewise indistinguishable for these two cases.

The overall impression one obtains from looking at the $\rho_n = \rho_p$ curves (the dotted lines in Figs. 9 through 12) is that they correspond to a diffraction pattern which is somewhat more compact, or squeezed together, than the data suggest. Such a general trend tends to mean that the diffracting object has been taken to be too large. Adjusted neutron distributions which yield somewhat better agreement with the data are in the direction to pull in the outer neutrons. This does indeed spread the diffraction patterns so that they become more like the observed patterns. In the adjusted ^{40}Ca neutron distributions there are approximately 20% fewer neutrons in the region beyond R_A. In the adjusted ^{208}Pb neutron distributions this percentage is similar.

For ^{208}Pb, where $N > Z$, a compression of the neutron density in the region beyond R_A does not necessarily mean that there are fewer neutrons than protons anywhere. In order to illustrate this point, we show the ratio $R = \rho_n/\rho_p$ in Fig. 8. The straight line at $R = 1.537$ indicates the ratio N/Z=126/82, and wherever R is greater than unity, there is an excess of neutrons at that radius. The solid line represents the HFB result, in which the distribution of neutrons follows closely that of the protons. The dash-dotted curve is greater than unity until $r = 7.3$ fm, showing that here the neutrons though depleted compared to the HFB case are still in excess of the protons, except at very large radii, where there are essentially no particles present.

Elastic scattering observables for protons on ^{40}Ca at 200 and 500 MeV are shown in Figs. 9 and 10. The data appear in Figs. 9(a) and 10(a). The solid curves in these figures represent the calculations with the HFB neutron distributions. The dash-dotted line is our "best" adjustment of the neutron distribution in ^{40}Ca. This distribution is shown in Fig. 6. Other neutron distributions are also displayed in Fig. 6 and the corresponding scattering observables are compared in the (b) panels. The separation into (a) and (b) parts is solely because otherwise our figures became too crowded. In Figs. 9(b) and 10(b), we see the sensitivity to the changes in the neutron density. Comparison of these results with the distributions

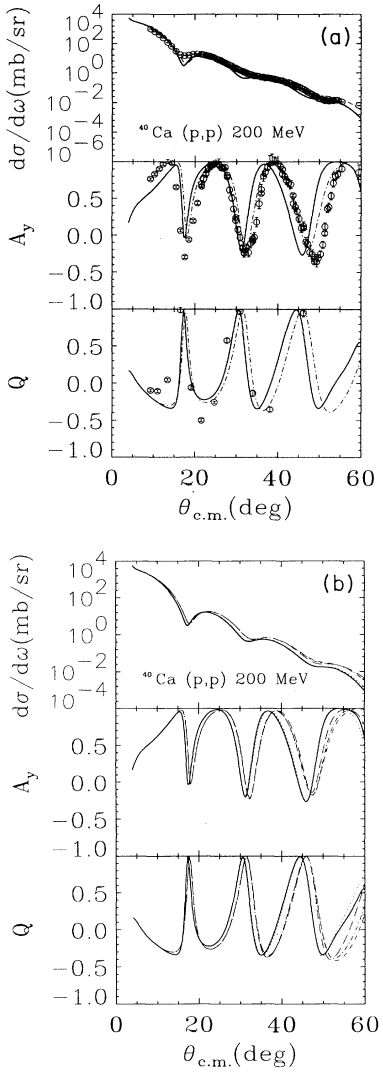

FIG. 9. (a) The observables σ, A_y, and Q for elastic proton scattering from ^{40}Ca at 200 MeV laboratory energy. The calculations are performed with a first-order optical potential in the Watson formulation obtained from the full Bonn interaction in the optimum factorized form. The solid curve represents the calculation with a neutron density obtained from an HFB calculation; the dash-dotted curve employs the neutron density of case (b) in Fig. 6. The proton density is taken from a 24 parameter Sum-of-Gaussian fit to electron scattering data [10]. The experimental data are from Ref. [24]. (b) Same as for (a). The solid curve employs a neutron density from a microscopic HFB calculation, whereas the short-dashed, dash-dotted, and long-dashed curves represent calculations with the neutron densities defined as cases (a), (b), and (c) in Fig. 6. The dotted line represents a calculation with $\rho_p = \rho_n$.

in Fig. 6 clearly shows the insensitivity to the interior region. In Table I we give the rms radii corresponding to the distributions shown in Figs. 6 and 7. The insensitivity to the interior region is reflected in this table, where we see that distributions similar in the surface region, which yield similar results for the observables, may have different rms radii.

Elastic scattering observables for protons on ^{208}Pb at 200 and 500 MeV are shown in Figs. 11 and 12. The data appear in Figs. 11(a) and 12(a). The solid curves in these figures represent the calculations with the HFB neutron distributions. The dash-dotted line is our "best" adjustment of the neutron distribution in ^{208}Pb. This distribution is shown in Fig. 7. Other neutron distributions for ^{208}Pb are also displayed in Fig. 7 and the corresponding scattering observables are compared in the (b)

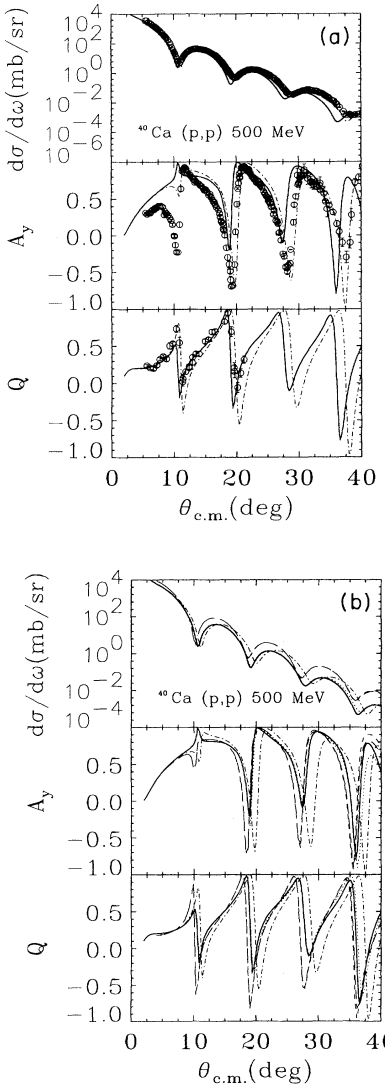

FIG. 10. (a) The observables σ, A_y, and Q for elastic proton scattering from ^{40}Ca at 500 MeV laboratory energy. The meaning of the curves is the same as in Fig. 9(a). The experimental data are from Ref. [25]. (b) Same as for (a). The curves have the same meaning as in Fig. 9(b).

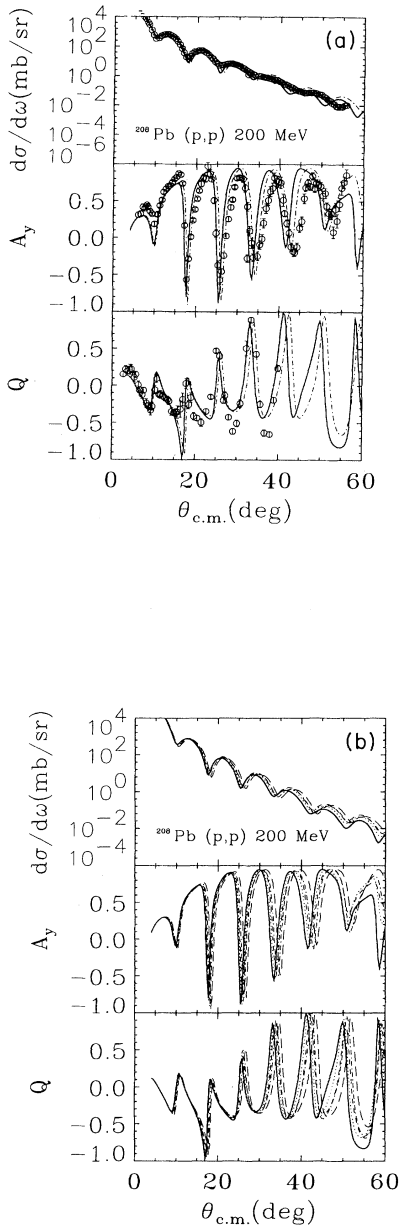

FIG. 11. (a) The observables σ, A_y, and Q for elastic proton scattering from ^{208}Pb at 200 MeV laboratory energy. The calculations are performed with a first-order optical potential in the Watson formulation obtained from the full Bonn interaction in the optimum factorized form. The solid curve represents the calculation with a neutron density obtained from an HFB calculation; the dash-dotted curve employs the neutron density of case (b) in Fig. 7. The proton density is taken from a 24 parameter Sum-of-Gaussians fit to electron scattering data [22]. The experimental data are from Ref. [26]. (b) Same as for (a). The solid curve employs a neutron density from a microscopic HFB calculation, whereas the short-dashed, dash-dotted, and long-dashed curves represent calculations with the neutron densities defined as cases (a), (b), and (c) in Fig. 7. The dotted line represents a calculation where the neutron density is taken to be the scaled proton density.

panels. We note that the dotted curve in Fig. 7 represents the proton distribution (normalized to Z protons), whereas the dash-dot-dotted line represents the same distribution multiplied by N/Z (normalized to N neutrons). Of course, it is a distribution so rescaled, to which we refer, when we say $\rho_n = \rho_p$. In Figs. 11(b) and 12(b) we see the sensitivity to changes in the neutron density. Once again we observe the insensitivity to the interior region. We note that for the long-dashed curve in Fig. 11(b) the compression of the diffraction pattern is somewhat greater than the data call for. This is the only case in Fig. 8, where R falls below unity. This suggests that although the neutrons are pulled in relative to the protons there is nevertheless always an excess of neutrons at all radii in ^{208}Pb. Neutron rms radii for these distributions are displayed in Table I.

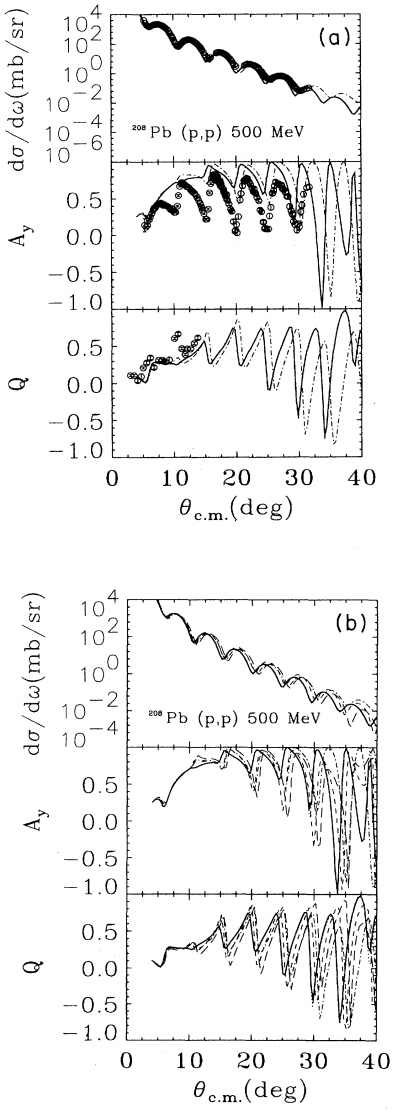

FIG. 12. (a) The observables σ, A_y, and Q for elastic proton scattering from ^{208}Pb at 500 MeV laboratory energy. The meaning of the curves is the same as in Fig. 11(a). The experimental data are from Ref. [25]. (b) Same as for (a). The curves have the same meaning as in Fig. 11(b).

TABLE I. The rms radii in fm for the neutron and proton distributions of ^{40}Ca and ^{208}Pb. The different cases are discussed in the text.

Case	^{40}Ca		^{208}Pb	
	rms (n)	rms (p)	rms (n)	rms (p)
$\rho_n = \rho_p$	3.479	3.479	5.503	5.503
HFB	3.379		5.572	
(a)	3.050		5.438	
(b)	3.033		5.238	
(c)	3.044		5.015	

Neutron rms radii for these distributions are displayed in Table I.

There still remain many unresolved issues before proton elastic scattering can be used accurately to determine target neutron distributions. The present analysis does suggest that the surface neutrons are pulled in somewhat relative to the protons. This is in sharp contradiction to the HFB predictions, in which the neutrons and protons are distributed similarly.

A further indication of the relative compression of the surface neutrons may lie in the variational calculations of the ground state of ^{16}O by Pieper *et al.* [23], who obtain a smaller rms radius for ^{16}O than the electron scattering measurements indicate. Since this calculation does not distinguish neutrons from protons, it may suggest that their radius is closer to the neutron radius, and that the inclusion of the Coulomb repulsion would indeed lead to a separation such as we see here. Without further study of the neglected effects implicit in the first-order multiple scattering calculations presented here, no firm conclusions regarding the neutron distributions can be drawn.

IV. SUMMARY AND CONCLUSION

The treatment of the isovector degrees of freedom is included in the framework of the correct first-order Watson multiple scattering series. The construction of the steps required are presented and discussed. Results comparing elastic proton scattering from ^{40}Ca and ^{208}Pb are shown to reflect sensitivities to isovector degrees of freedom. Adjustments to the neutron density distribution emphasize such sensitivities. Changes to the neutron density may be indicated by comparisons of theoretical predictions with elastic proton scattering angular distribution data, which favor a smaller neutron rms radius and a thinner surface. It remains unrealistic to expect to be able to extract detailed quantitative information about the target nucleus from elastic proton-nucleus reactions.

ACKNOWLEDGMENTS

This work was performed partially under the auspices of the U. S. Department of Energy under Contract

No. DE-FG02-93ER40756 and by the Lawrence Livermore National Laboratory under Contract No. W-7405-ENG-48. One of the authors (C.R.C.) would also like to acknowledge the gracious hospitality of the Service de PTN at the CEA/Bruyères-le-Châtel, where part of this work was performed. The computational support of the Ohio Supercomputer Center under Grants No. PHS206 and No. PDS150 is gratefully acknowledged.

[1] R. Crespo, R.C. Johnson, and J.A. Tostevin, Phys. Rev. C **41**, 2257 (1990).
[2] H.F. Arellano, F.A. Brieva, and W.G. Love, Phys. Rev. Lett. **63**, 605 (1989); Phys. Rev. C **41**, 2188 (1990).
[3] Ch. Elster, T. Cheon, E.F. Redish, and P.C. Tandy, Phys. Rev. C **41**, 814 (1990).
[4] C.R. Chinn, Ch. Elster, and R.M. Thaler, Phys. Rev. **44**, 1569 (1991).
[5] R.W. Finlay, G. Fink, W. Abfalterer, P. Lisowski, G.L. Morgan, and R.C. Haight, in Proceedings of the International Conference on Nuclear Data for Science and Technology, Jülich, 1991 (unpublished).
[6] R. Kozack and D.G. Madland, Nucl. Phys. **A509**, 664 (1990).
[7] K. Kaki, Nucl. Phys. **A531**, 478 (1991).
[8] K.M. Watson, Phys. Rev. **89**, 575 (1953); N.C. Francis and K.M. Watson, *ibid.* **92**, 291 (1953).
[9] L. Ray, P.C. Tandy, and R.M. Thaler, Phys. Rev. C **28**, 506 (1983).
[10] I. Sick, J.B. Bellicard, J.M. Cavedon, B. Frois, M. Huet, P. Leconte, P. X. Ho, and S. Platchkov, Phys. Lett. **88B**, 245 (1979).
[11] S.J. Pollock, E.N. Fortson, and L. Wilets, University of Washington Report No. DOE/ER/40427-09-N92 (submitted to Phys. Rev. C).
[12] A. Kerman, M. McManus, and R.M. Thaler, Ann. Phys. (N.Y.) **8**, 551 (1959).
[13] M.A. Nagarajan, W.L. Wang, D.J. Ernst, and R.M. Thaler, Phys. Rev. C **11**, 1167 (1975).
[14] H. Garcilazo, Phys. Lett. **82B**, 32 (1979).
[15] See, for example, J.F. Berger, M. Girod, and D. Gogny, Nucl. Phys. **A502**, 85c (1989); J.P. Delaroche, M. Girod, J. Libert, and I. Deloncle, Phys. Lett. B **232**, 145 (1989).
[16] J.F. Berger, M. Girod, and D. Gogny, Comput. Phys. Commun. **63**, 365 (1991).
[17] A. Picklesimer, P.C. Tandy, R.M. Thaler, and D.H. Wolfe, Phys. Rev. C **30**, 2225 (1984).
[18] P.C. Tandy, E.F. Redish, and D. Bollé, Phys. Rev. C **16**, 1924 (1977).
[19] E.F. Redish and K. Stricker-Bauer, Phys. Rev. C **36**, 513 (1987).
[20] R. Machleidt, K. Holinde, and Ch. Elster, Phys. Rep. **149**, 1 (1987).
[21] Ch. Elster and P.C. Tandy, Phys. Rev. C **40**, 881 (1989).
[22] B. Frois, J.B. Bellicard, J.M. Cavedon, M. Huet, P. Leconte, P. Ludeau, A. Nakada, and P.X. Ho, Phys. Rev. Lett. **38**, 152 (1977).
[23] S.C. Pieper, R.B. Wiringa, and V.R. Pandharipande, Phys. Rev. C **46**, 1741 (1992).
[24] E.J. Stephenson, in *Antinucleon- and Nucleon-Nucleus Interaction*, edited by G. Walker, C.D. Goodman, and C. Olmer (Plenum, New York, 1985), p. 299.
[25] G.W. Hoffmann, L. Ray, M.L. Barlett, R. Fergerson, J. McGill, and E.C. Milner, Phys. Rev. Lett. **47**, 1436 (1981); A. Rahbar, B. Aas, E. Bleszynski, M. Bleszynski, M. Haji-Saeid, G.J. Igo, F. Irom, G. Pauletta, and A.T.M. Wang, *ibid.* **47**, 1811 (1981).
[26] D.A. Hutcheon *et al.*, in *Proceedings of the Fifth International Symposium on Polarization Phenomena in Nuclear Physics, Santa Fe, 1980*, edited by G.G. Ohlson, R.E. Brown, N. Jarmie, W.W. McNaughton, and G.M. Hale, AIP Conf. Proc. No. 69 (AIP, New York, 1981), p. 454.